Structural Behavior of Sandwich Beams with Flax Fiber-Reinforced Polymer Faces and Cardboard Cores under Monotonic and Impact Loads

Dillon Betts[1] S.M.ASCE, Pedram Sadeghian[2] M.ASCE, and Amir Fam[3] F.ASCE

ABSTRACT: To meet the ever-increasing demand for more environmentally conscious building designs, it is important that there are sustainable building material options available. Natural and recycled materials can be used in sandwich panels to reduce their environmental footprint. In this study, twelve sandwich beams constructed with flax fiber-reinforced polymer (FFRP) faces and recycled corrugated cardboard cores were studied experimentally under monotonic and impact loading. Each sandwich beam was 1200 mm long, 150 mm wide and was constructed of two-layer FFRP faces and a 75 mm thick corrugated cardboard core. Six specimens were prepared using a plain cardboard core and six with a waxed cardboard core. Two separate test methods were employed in this study: a three-point bending test and a drop weight impact test. Three specimens of each type with a span length of 1120 mm of each type were tested under monotonic load. The load was applied through a 150 mm wide steel hollow structural section (HSS) and was measured with a 250 kN load cell. The midspan deflection was measured with a string potentiometer and the strains in the top and

[1] PhD Candidate, Department of Civil and Resource Engineering, Dalhousie University, 5268 DaCosta Row, Halifax, NS B3H 4R2, Canada. Email: dillonbetts@dal.ca (corresponding author)
[2] Assistant Professor and Canada Research Chair in Sustainable Infrastructure, Department of Civil and Resource Engineering, Dalhousie University, 5268 DaCosta Row, Halifax, NS, B3H 4R2, Canada. Email: pedram.sadeghian@dal.ca
[3] Donald and Sarah Munro Chair Professor in Engineering and Applied Science and Associate Dean (Research and Graduate Studies), Department of Civil Engineering, Queen's University, Kingston, ON, K7L 3N6, Canada. Email: amir.fam@queensu.ca

bottom faces at midspan were measured using strain gauges. The monotonic test data was recorded at a rate of 10 Hz. Three specimens of each type were tested under a drop weight impact load. The drop weight was applied to the midspan. To match the monotonic tests, the drop weight was affixed with a 150 mm HSS section loading surface. The midspan displacement was measured with a fast-action string potentiometer and the midspan face strains were measured using strain gauges. The impact data was recorded at a rate of 25 kHz. Additionally, a high-speed video (500 frames per second) was taken of each impact test. The residual monotonic flexural behavior after impact was also investigated for specimens that survived the impact testing (that is, they were additionally tested under monotonic three-point bending). The results of the tests were compared with the results of similar tests on sandwich beams with conventional petroleum-based foam cores and showed that the cardboard core beams behaved similarly to the foam core beams. It was determined that core manufacturing and specimen preparation had a significant effect on the overall specimen behavior and potentially caused premature failure in some of the tests. The residual monotonic tests of specimens after impact showed that there was no significant reduction in specimen strength or stiffness after an impact event. Existing models used for predicting the behavior of foam-core FFRP-sandwich beams were used to predict the behavior of the cardboard specimens tested in this study.

KEYWORDS: Sandwich Structures, Natural Materials, Flax, Cardboard, Sustainable Infrastructure

INTRODUCTION

With climate change being one of the major issues faced by society, it is important that new infrastructure is designed with environmental consciousness in mind. The use of natural materials, such as plant fibers in natural fiber-reinforced polymer (FRP) composites, is one method of increasing the environmental sustainability of building structures (Bensadoun et al. 2016; Christian and

Billington 2011; Mak et al. 2015). Flax-FRP (FFRP) composites have gained popularity due to their comparatively high strength and stiffness (Ramesh et al. 2017) and the commercial availability of flax fabrics. To further increase the environmental sustainability of FFRPs, they can be fabricated using thermoset resins with high bio-contents (Betts et al. 2018b; Mak et al. 2015). While flax fibers have been shown to be weaker than traditional synthetic fibers, such as glass or carbon, they are biodegradable have a comparable modulus-weight ratio when compared to E-glass fibers (Mallick 2007). They also have a lower embodied energy and can be used in situations where the high strength of the synthetic FRPs have been shown to be underutilized, such as in sandwich panels where the strength of the core material often governs. (Betts et al. 2018b; Codyre et al. 2016; Mak et al. 2015).

Sandwich structures are used when a relatively high strength and stiffness and light weight are required, such as building envelopes (Allen 1969; Fam and Sharaf 2010; Nguyen et al. 2005; Sharaf et al. 2010; Torre and Kenny 2000; Triantafillou and Gibson 1987). Sandwich structures have also been used in applications such as for floor slabs (Ferdous et al. 2019; Zhu et al. 2018), structural beams (Ferdous et al. 2018a) and railway sleepers or ties (Ferdous et al. 2018b). Sandwich structures typically have two main elements: the structural faces and the lightweight core. The core is used to resist shear forces and to separate the two faces to provide a large moment of inertia to resist flexural loading. For applications where high insulative properties are required, synthetic materials such as foam are used for the core; but when insulation is not a requirement, researchers have used natural core materials, such as cork (Boria et al. 2018; Sadeghian et al. 2018), or recycled materials, such as corrugated cardboard (Betts et al. 2019; McCracken and Sadeghian 2018; Pflug et al. 2000, 2002).

In Canada, nearly 100% of new cardboard is made from recycled materials and it is 100% biodegradable (McCracken and Sadeghian 2018; Paper & Paperboard Packaging Environmental Council 2017) making it an environmentally sustainable alternative for the traditional synthetic core materials. Because of its environmental sustainability, corrugated cardboard has been investigated for use in temperature and sound attenuation applications (Asdrubali et al. 2016; Secchi et al. 2016) as well as structural applications in small buildings (El Damatty et al. 2000) and concrete slabs (Fraile-Garcia et al. 2019). One obvious potential limitation for the use of corrugated cardboard as a core material is its susceptibility to moisture absorption which can lead to reduced capacity and permanent damage. In situations where cardboard could be exposed to high amounts of moisture, cardboard manufacturers protect the cardboard by applying a layer of wax after manufacturing. There is the potential to use this waxed cardboard as cores for sandwich panels where there is increased risk to moisture exposure. Another limitation is the low fire resistance of these structures. However, even with this limitation, these structures are potentially suitable for use as non-fire rated wall partitions in buildings due to their light weight, environmental-friendliness and aesthetic appeal.

Another potential application for these sandwich structures is non-load bearing building enclosures or cladding systems. These enclosure systems are primarily loaded in the lateral direction due to wind and air pressure and therefore it is important to understand their flexural behaviour. For this reason, sandwich structures have been examined under flexural loads (Codyre et al. 2016; Ferdous et al. 2018a; Manalo et al. 2016; Petras and Sutcliffe 1999; Sadeghian et al. 2018; Sharaf and Fam 2012; Vitale et al. 2017). Additionally, during storm events, building exteriors can be subject to impact loads from flying debris during storm events. Therefore, it is also important to understand the impact behavior of the panels and the residual properties after an impact event and as such sandwich structures have been studied extensively under impact loads (Anderson and Madenci 2000; Atas and Potoglu 2016; Betts et al. 2018a; Chai and Zhu 2011; Plagianakos and Papadopoulos 2014; Schubel et al. 2005; Torre and Kenny 2000; Zhu and Chai 2013) and air blast loads (Andrews and Moussa 2009) .

The currently available research on sandwich panels with cardboard cores has focused on small-scale specimens with plain cardboard cores under static loads (McCracken and Sadeghian 2018; Pflug et al. 2000, 2002). There remains a gap in the research on the performance of large-scale sandwich beams with FFRP faces and natural or recycled cores under static loads and especially on their behavior under impact loads. It is important to understand the behavior of large-scale panels as they more accurately represent the behavior of actual structures. Large scale tests also remove the potential for size effects to influence the test results, especially under impact loads. In the current study, large-scale sandwich beams constructed with plain and waxed corrugated cardboard cores and FFRP faces were fabricated and tested under monotonic, impact and post-impact residual monotonic loads. The aim of the current study is to show that these panels have the required strength and impact resistance to act as wall partitions in buildings. Additionally, through the use of the waxed cardboard cores with higher resistance to moisture absorption, these panels also have potential for use in applications with more exposure to moisture, such as in building cladding systems. Finally, an existing model developed for similar large-scale sandwich beams with FFRP faces and foam cores was used to accurately predict the monotonic behavior of the beams in the current study.

RESEARCH SIGNIFICANCE

As the effects of climate change become increasingly evident, it is important that engineers and designers consider the environmental impact of new infrastructure designs. This research provides new information to the field of sustainable infrastructure design through the testing and analysis of building materials comprised of natural and recyclable materials. The use of natural materials, such as flax fibers, for the construction of sandwich structures with foam cores has been studied in the recent past (Betts et al. 2018b; Codyre et al. 2016; Mak et al. 2015; Mak and Fam 2019; Sadeghian et al. 2018). To further increase the sustainability of these structures, the current study is examining a more sustainable alternative for the core material in the form of corrugated cardboard, which is both recyclable and biodegradable. While the potential limitations of using cardboard as a core material are recognized, there are applications for sandwich structures with these cores, especially as non-fire-rated wall partitions. The aim of this study is to provide test data and analysis methods for the use of biodegradable sandwich panels for use in environmentally sustainable structural and architectural design of buildings. These panels could especially be used as part of new environmentally sustainable structures and innovative construction projects. This paper presents the test data of these sandwich panels under monotonic loads and impact loads and shows that they can be accurately analysed using a simplified procedure which makes structural and architectural design using these structures feasible.

EXPERIMENTAL PROGRAM

In this section, the experimental program is discussed. First, the test matrix is presented, and the naming convention is explained. The materials used are described and the specimen fabrication procedure is discussed at length. Finally, the test set-ups and procedures are presented.

Test Matrix

Twelve sandwich beams with cardboard cores and FFRP faces were tested: six specimens with plain cardboard cores and six with waxed cardboard cores. Each specimen was 1200 mm long, 150 mm wide and approximately 80 mm thick. The specimens were constructed of two-layer FFRP faces and 75 mm thick corrugated cardboard cores. Three specimens of each type were tested under monotonic three-point bending and three of each type were tested under a drop weight impact at midspan. The monotonic tests were performed first, and the first drop height of the impact tests was based on the results of the static tests. The naming convention for the specimens was as follows: [P/W]C-[S/D]-X, where P is plain, W is waxed, S is static, D is dynamic, and X is a sequential number used to distinguish identical specimens. The test matrix is presented in Table 1.

Materials

The FFRP faces were fabricated using a bio-based epoxy resin and a balanced bidirectional flax fabric. The resin matrix was bisphenol A epoxy with a reported tensile strength and modulus of 53.2 MPa and 2.65 GPa, respectively and a compressive strength of 77.9 MPa (Entropy Resins 2013a, 2015). This resin was used for the fabrication of the FFRPs as well as the connection between the faces and core. It should be noted that the reported strength and modulus are based on using the epoxy matrix with a fast-setting hardener (Entropy Resins 2013a). For the current project, a longer pot life was required and therefore a slow-setting cycloaliphatic polyamine hardener was used (Entropy Resins 2013b). Therefore, to understand of the constitutive behavior of the FFRP matrix material the epoxy-hardener combination used in this study was tested under uniaxial tension. The tensile strength and modulus of the epoxy mixed with the slow-setting hardener were tested and measured to be 57.9 MPa and 3.20 GPa, respectively (Betts et al. 2018b). The flax fabric used was a balanced bidirectional 2x2 twill fabric with a reported areal mass of 400 g/m^2, which was measured to be 410 g/m^2.

The properties of the FFRPs used in this study were investigated previously by Betts et al (Betts et al. 2018b). The tensile strength, modulus and elongation of the FFRP faces were found to be 45.4 MPa, 7.51 GPa and 0.0083 mm/mm, respectively. Betts et al (2018b) used a novel test method to determine the properties of the FFRPs in compression. The compressive modulus was found to be 6.73 GPa and ultimate strength and corresponding strain were found to be 86.4 MPa and 0.0327 mm/mm, respectively.

Two types of cardboard were supplied by a local manufacturer for this study: plain corrugated cardboard and waxed corrugated cardboard. For each type of cardboard, ten random samples were selected, and their properties measured. The plain cardboard strips used had an average thickness of

4.1 mm and an average density of 127 kg/m^3. The waxed cardboard strips used had an average thickness of 4.1 mm and an average density of 166 kg/m^3.

Specimen Fabrication

To construct the sandwich beams, the first step was the manufacturing of the core. Each plain cardboard core was created by adhering multiple strips of cardboard together, as shown in Figure 1, to achieve the required specimen width. The strips were provided by the cardboard manufacturer and adhered using the same glue used in the manufacturing of the cardboard. As shown in Figure 1a, two rails were fastened to a worktable at right angles. The first strip of plain cardboard was placed firmly against each rail by hand. For each subsequent strip, a small amount of glue was applied before placement next to the previous strip as show in Figure 1b. The fabrication of the waxed cores was altered slightly because the glue did not cure as quickly, which allowed it to migrate downwards before curing. Therefore, the waxed strips were stacked vertically as opposed to horizontally. That is, that the first strip of waxed cardboard was placed flat on the table surface and glue was applied to the top face. Each subsequent strip was then placed on top of the previous strip.

After all cardboard strips were placed (i.e. such that the overall width was 150 mm), weights were placed against the core and glue while allowed to cure. This is shown in Figure 1c. Once the glue had cured, the top and bottom surfaces of the cardboard cores were sanded to create a flat surface for applying the FFRP faces as shown in Figure 1d. As will be discussed further in the results section of this paper, this part of the fabrication procedure is vital to ensure a secure bond between the core and faces. The densities of the plain cardboard cores and waxed cardboard cores were 136 kg/m^3 and 174 kg/m^3 respectively.

The faces were made using a wet lay-up procedure. First, a layer of parchment paper was placed on a flat work surface. Once the work surface was prepared, the bio-based epoxy was mixed with slow-set hardener. A layer of the mixed epoxy was applied to the parchment paper to cover the area of the flax fabric, which was 600 mm wide and 1200 mm long, and a layer of flax fabric was placed on the wetted section of parchment paper. A plastic scraper was then used to push out any air from under the placed section of flax fabric. This was done by pushing the plastic scraper longitudinally along fabric in one direction, which also worked to soak the fabric in resin layer below. Then, a second layer of epoxy was applied to the surface of the flax fabric and another layer of flax fabric was placed and smoothed with a plastic scraper as described above. The surface of the fabric was then wetted with another layer of epoxy and three cardboard cores were placed on the wetted surface as shown in Figure 1e. The face was allowed to cure at room temperature for seven days at which point the entire procedure was completed again for the second face. It should be noted that the curing took place in a ventilated air-conditioned room. Once the second face was cured, the specimens were cut out using a band saw and all cut edges were sanded smooth.

Test Setup and Instrumentation

As a part of this study, two types of tests were performed: static tests and impact tests. For both tests, the load/impact was applied at the midspan through a 150 mm wide loading surface made from a steel hollow structural section (HSS) to mitigate the local failure mechanisms, such as indentation. The specimens were instrumented with strain gauges on the top and bottom faces at midspan as well as a connection point for a string potentiometer on the bottom face at midspan. For both tests, the same fast-action string potentiometer was used.

Monotonic Tests

The procedure for ASTM D790 (ASTM 2017) was adopted for these tests, with some changes, such as the width and shape of the loading surface. All details for the tests are shown in the three-point bending test set-up presented in Figure 2. Both supports were roller type supports. The test frame used was bolted to a concrete strong floor. An actuator with a load cell attached applied load to the specimen through a 150 mm wide HSS. All data was sampled at a rate of 10 Hz.

Impact Tests

The impact test set-up is presented in Figure 3. In order to directly compare the impact tests with the monotonic tests and to observe the one-way bending during impact of the panels, almost the same test set-up was used as in the monotonic tests. For the design of the drop weight frame and test, ASTM D7136 (ASTM 2005) was adopted where applicable. A 10.4 kg weight was used to impact the specimens at midspan in a self reaction test frame. The first drop height was determined based on the average energy that caused failure in monotonic tests of all specimens. Then, based on the performance of the first drop test, the subsequent drop heights were selected. This will be discussed in detail in the results section of this paper. As shown in Figure 3, each sandwich beam was simply supported by one pin-type support and one roller support. At both supports, an upper fixture was used to stop specimens from lifting off supports after impact. An accelerometer was attached to the drop weight. All data was sampled at a rate of 25 kHz. A 25 mm diameter hole was cut into the center of HSS impact surface to ensure that the top face strain gauge was not damaged during the impact.

RESULTS AND DISCUSSIONS

In this section the experimental and analytical results are discussed. The behavior of the specimens under monotonic three-point bending are presented and the effect of waxing the core is examined. Then, the use of design-oriented model developed by Betts et al. (2018b) for sandwich panels with foam cores is used to examine its applicability to predict the behavior of cardboard core FFRP-sandwich beams. The behavior of the specimens under a single impact event is presented and discussed. After the impact event the specimens were tested to determine their post-impact residual strength. The results of these tests are presented and compared to the results of the monotonic test results of the intact specimens.

Monotonic Behavior

The results of the monotonic three-point bending tests are presented in Table 2 and a photo of the failed specimens is presented in Figure 4. As shown in Table 2 there is a high variance in the maximum loads sustained by identical sandwich beam specimens. The maximum load results of the plain core specimens and waxed core specimens had coefficient of variation (CV) of 22% and 47%, respectively. The load capacity was greatly affected by the strength of the connection between the faces and core, specifically on the compression face. This was evidenced by the failure modes observed during the tests.

Failure Modes

Figure 4 shows each specimen after testing and the failure of each specimen. All statically tested specimens failed by compression face wrinkling save 2FL-WC-S-3 which failed due to core shear. As shown in Table 2, this specimen exhibited the highest peak load. This indicates that if the connection between the face and core could be improved, the failure load could be increased for specimens that failed in compression wrinkling. The compression wrinkling could be considered as a premature failure of these specimens and highlights the importance of the connection between the face and core. The authors believe that the separation between the compression face and the core was due to an increase of tensile stresses between the two layers as the compression face buckles away from the core. To resist this compression face wrinkling there needs to enough surface area between the face and core to withstand the tensile stresses developed at the interface. Therefore, in future studies, additional measures should be implemented to improve the interface between the core and faces, such as: the use of a plane flatten the surface of the cardboard cores and the use of a veil to provide more area for the adhesive between the face and the core.

Load-Deflection Behavior

Figure 5a shows the load-deflection results of the static tests. From the plot, it can be seen that the specimens exhibited a nonlinear load-deflection behavior before ultimate failure. Table 2 shows the results of the tests. Note that the specific strength of the beams was calculated by dividing the ultimate load by the specimen mass within the span length. The stiffnesses shown in Table 2 were calculated by applying a linear fit of the data between a load of 0 kN and 1.5 kN, which is within the first linear portion of all tested specimens, as seen in Figure 5a. Table 2 shows that the average stiffness of the WC specimens is 361.2 ± 25.8 N/mm, which is 41% higher than the PC specimens which have an average stiffness of 256.9 ± 18.2 N/mm. However, due to the high variability of the data, there was no significant difference in the peak loads or specific strengths sustained by specimens with different core types.

Moment-Curvature Behavior

Figure 5b shows the moment-curvature behavior of the static tests. All specimens exhibited a nonlinear moment-curvature relationship. By examining the plot and the results presented in Table 2, it can be seen that the flexural rigidities of the sandwich beams are not significantly affected by the core type. The average flexural rigidity of the WC specimens was 12.74 ± 1.06 kN-m^2 and the average flexural rigidity of the PC type specimens was 11.96 ± 2.00 kN-m^2. The flexural rigidities were determined by fitting a line to the first linear portion of the plots between a moment of 0 kN-m and 0.3 kN-m. As the moment was calculated based on the load, there is also no significant difference in the moment capacity of the beams, as discussed above.

Modelling

The load-deflection and moment-curvature plots for all specimens were nonlinear. In a previous study, Betts et al. (2018b) attributed this nonlinear behavior to the intrinsic nonlinear behavior of the FFRP faces. They presented a design-oriented model to predict the load-deflection and moment-curvature behavior of sandwich beams with nonlinear FFRP faces and foam cores under three-point and four-point bending. Numerous authors have noted the approximately bilinear behavior of FFRPs and other natural fiber FRPs (Bensadoun et al. 2016; Betts et al. 2018b; Christian and Billington 2011; Hristozov et al. 2016; Mak et al. 2015; Sadeghian et al. 2018). Through preliminary testing of flax fibers and their composites, Betts et al. (2017, 2018c) have shown that the nonlinearity of FFRPs is likely due to the behavior of the flax fibers. Therefore, the model by Betts et al. (2018b) assumes that the faces act in a bilinear fashion which in turn causes a bilinear behavior of the sandwich panels. The same face material used in the study by Betts et al. (2018b) was used in the current study and therefore the same bilinear model was adopted for the faces. The model allows the user to find the stiffness and strength of the sandwich beams. Some authors in this field have performed tests on sandwich beams with multiple spans and were able to determine the shear modulus (Ferdous et al. 2017; McCracken and Sadeghian 2018). However, with only one span length in these tests, this was not possible for these tests.

The model assumes that the FFRP faces in a perfectly bilinear fashion and that the neutral axis is located approximately at the midplane (Betts et al. 2018b). The primary and secondary moduli are determined using Eq. 1 and Eq. 2.

$$E_{f_1} = \frac{1}{2}(E_{f_t} + E_{f_c}) \quad (1)$$

$$E_{f_2} = \frac{1}{2}(\frac{2}{3}E_{f_t} + \frac{2}{5}E_{f_c}) = \frac{1}{3}E_{f_t} + \frac{1}{5}E_{f_c} \quad (2)$$

where E_{f1} is the initial modulus, E_{f2} is the secondary modulus, E_{ft} is the initial tensile modulus and E_{fc} is the initial compression modulus.

The load-deflection behavior based on two points: a “point-of-transition” where the FFRP changes from its initial modulus to its secondary modulus and the ultimate point, where the ultimate strain of the FFRP is reached. The point-of-transition load and deflection can be calculated using Eq. 3 and Eq. 4, respectively, and the ultimate load and deflection can be determined using Eqs. 5-7 (Betts et al. 2018b, 2020).

$$P_0 = \frac{4tbdE_{f_1}\epsilon_{f_0}}{L} \tag{3}$$

$$\Delta_0 = \frac{L^2}{6d}\epsilon_{f_o} + \frac{P_0 L}{4G_c(\frac{bd^2}{c})} \tag{4}$$

$$P_u = \frac{4tbd[E_{f_1}\epsilon_{f_0} + E_{f_2}(\epsilon_{f_u} - \epsilon_{f_0})]}{L} \tag{5}$$

$$\Delta_u = \frac{L^2}{12d}\left[(1+\lambda)\epsilon_{f_0} + \left(2-\lambda-\lambda^2\right)\epsilon_{f_u}\right] + \frac{P_u L}{4G_c(\frac{bd^2}{c})} \tag{6}$$

where t is the thickness of the FFRP faces, b is the beam width, d is the distance between the face centroids, ϵ_{fo} is the strain at the point-of-transition determined by Betts et al. (2018b) to be 0.0018 mm/mm, ϵ_{fu} is the ultimate tensile strain of the FFRPs, L is the span length, G_c is the shear modulus of the core and λ is a parameter found using Eq. 7.

$$\lambda = \frac{1}{2 + 2\frac{E_{f_2}}{E_{f_1}}\left(\frac{\epsilon_{f_u}}{\epsilon_{f_0}} - 1\right)} \tag{7}$$

The corresponding moments can be found by simply converting the loads to moments using the relation for three-point bending, $M_i = P_i L / 4$. The corresponding curvatures can be found simply by $\psi_i = 2\epsilon_i / d$. After the general model has been developed the failure loads are found by using the procedure presented by Triantafillou and Gibson (1987) and subsequently used by Betts et al. (2018b).

The cardboard core material used in this study does not have data available. However, the same C-type flute cardboard was used by McCracken and Sadeghian (2018) and through their tests, they determined an approximate shear modulus (G_c) of 121.9 MPa. However, the compressive modulus and shear strength are unknown. To allow for modelling, these values were assumed based on the shear modulus by examining the relationship between the same properties of the foam cores used in the study by Betts et al. (2018b). It was found that the compressive modulus of the foams was typically 2.5 times that of the shear modulus and that the shear strength of the foams was typically 0.075 times that of the shear modulus of the foams. Therefore, in this study, the compressive modulus of the cardboard was assumed to be $E_c = 2.5G_c$ and the shear strength was assumed to be $\tau_{cu} = 0.075G_c$.

The results of the model are presented in Figure 5 and Table 3. The model is able to predict the load-deflection behavior of the sandwich beams well as presented in Figure 5a. The stiffness predicted by the model was 262.3 N/mm compared to the average stiffness of the PC specimens of 256.9 N/mm, a difference of less than 2.5%. However, the model overpredicts the ultimate load capacity and ultimate deflection with PC test-to-model ratios of 0.82 and 0.88, respectively. The moment-curvature model shown in Figure 5b captures the behavior of the beams well, however, it slightly underpredicts the initial flexural rigidity (*EI*, initial slope of the plot). As shown in Table 3, the PC test-to-model ratio of the flexural rigidity is 1.49.

Impact Behavior

The results of the impact tests are presented in Table 4 and the tested specimens are shown in Figure 4. The impact data was sampled at a rate of 25 kHz and included the strain in the top and bottom face at midspan and the specimen displacement at midspan. These specimen displacement measurements were used to calculate the specimen damping ratio, ξ, and specimen stiffness, K.

To determine the damping ratio, the damped period of each specimen was needed. This was found by measuring the average time between the local maxima and minima displacements during free vibration. The damped angular frequency was then calculated using Eq. 8.

$$\omega_d = \frac{2\pi}{T_d} \quad (8)$$

where ω_d is the damped angular frequency and T_d is the damped period of the structure. To find both the natural angular frequency and damping ratio, the exponential equation, Eq. 9, was used.

$$f(t) = Ae^{Bt} = Ae^{\xi \omega_n t} \quad (9)$$

where ω_n is the natural angular frequency and A and B are constants solved by fitting the exponential equation to both the maxima or minima displacement measurements during free vibration, as shown in Figure 6. Using the value of B determined this way, the natural angular frequency and damping ratio were solved by iterating Eq. 10 and Eq. 11 until the natural angular frequency converged to within 1%. To begin the iteration ω_n was assumed to be ω_d.

$$\xi = \frac{B}{\omega_n} \quad (10)$$

$$\omega_n = \frac{\omega_d}{\sqrt{1-\xi^2}} \quad (11)$$

In this study, the procedure was completed twice: once fitting the equation to the maxima displacements and once fitting the equation to the minima displacements. Then, the damping ratio and natural angular frequency were taken as the average of the two results. The specimen stiffness was then calculated as follows:

$$K = \frac{{\omega_n}^2 \, mL}{2} \quad (12)$$

where m is the specimen mass per unit length and L is the span length.

Impact Energy

For both the PC and WC type specimens, the first impact was based on the average energy to cause failure in all the monotonic tests, which was found to be approximately 62.7 J. Both PC and WC type specimens were able to resist the impact of 62.72 J (i.e. a drop height of 614 mm with a drop weight mass of 10.413 kg). The next impact test for both PC and WC type specimens was then performed at an energy of 109.81 J, a 75% increase from the first impact. The PC type specimen failed at this impact level and therefore the remaining specimen was tested at 86.32 J, the average of the first two impact test energy levels. The WC type specimen resisted the impact energy of 109.81 J and the remaining specimen was tested at an energy level of 154.96 J, an increase of approximately 150% from the initial impact of 62.72 J. The WC specimen failed at this impact level.

Because the types of structures are often used where reduced weight is a design requirement, an important property is the specific absorbed energy (SAE). The SAE of each specimen is presented in Table 4. Due to the lack of test data available, the ultimate SAEs of these beams are still unknown, but it can be concluded from these tests that the SAE of the WC and PC specimens is at a minimum 33.07 J/kg and 31.39 J/kg, respectively.

Strain and Displacement

Both strain and displacement at midspan were measured throughout the impact event. Sample test results of specimen 2FL-PC-D-1 are presented in Figure 7. This figure shows that after the impact event, there is a period of free vibration and that the drop weight was allowed to rebound during the tests. During the impact tests causing failure, there was no significant displacement data to report as the specimen failure caused the string potentiometer to disconnect. However, the energies resisted by both specimens caused deflections greater than those experienced during monotonic testing. The PC specimen impacted by 86.32 J deflected 23.3 mm compared to an average of 20.9 mm during the monotonic tests and the WC specimen impacted by 109.81 J deflected 25.6 mm compared to an average of 23.5 mm during the monotonic tests. These high levels of deflection indicate that the specimens were potentially close to their ultimate capacity during these impact tests. This is also supported by the fact that the maximum strains at these impacts in the bottom face exceeded the average ultimate FFRP tensile strain of 0.0083 mm/mm.

Residual Behavior After Impact

Specimens that did not fail during impact testing were tested under monotonic loading to determine post-impact residual properties. The results of these tests are presented in Figure 8 and Table 5. The tested specimens are presented in Figure 4.

Failure Mode (comparison with monotonic)

All residually tested specimens failed due to compression face crushing (CC), which is a face material failure mechanism. This contrasts the behavior exhibited by the monotonic tests of the intact specimens, five of which failed due to an interface stability failure between the core and face. All the residually tested specimens also resisted a larger ultimate load than their intact counterparts. These two facts indicate that either the intact specimens failed prematurely or that there is some phenomenon causing an increase in strength after an impact event. In previous tests of sandwich panels with FFRP faces and polyisocyanurate foam cores performed by the authors, a similar increase was observed during residual testing which suggests that there is an unknown condition causing this increase in strength and stiffness. Currently, it is suspected that this increase in strength and stiffness after impact is caused by a densification of the core material under the impact. However, this phenomenon is not yet fully understood and requires further detailed investigation. Future work to investigate this behavior will include removing sections of the core material from under the impact area of tested sandwich specimens and comparing the results with the behavior of intact core materials.

Additionally, the hysteretic behavior of the FFRP faces will be examined through further tension and compression testing. This will show the behavior of the FFRPs after prior loading and unloading, such as after an impact event.

Load-Deflection Behavior (comparison with monotonic)

The load-deflection and moment-curvature behavior of the residual tests are compared to the intact monotonic tests in Figure 8. The results of the residual tests are presented in Table 5. As discussed previously, the residual PC specimens and residual WC specimens resisted higher ultimate loads than their intact counterparts. The average ultimate load resisted by residual PC specimens was 6.25 kN which is an increase of 60.7% from the 3.89 kN resisted by intact PC specimens. Likewise, the residual WC specimens resisted an average ultimate load of 6.72kN, a 69.7% from the 3.96 kN resisted by the intact WC specimens. By examining Figure 8a and Figure 8c, the stiffnesses of both WC and PC type specimens were not affected by the impact event. The average stiffness of the residual PC specimens was 276.6 N/mm, which is within 7.7% of the average stiffness of the intact PC specimens. Likewise, the stiffness of the residual WC specimens was within 4.5% of the WC intact specimens.

Moment-Curvature Behavior (comparison with monotonic)

By examining Figure 8b and 8d, it can be seen that the moment-curvature behavior of the beams was affected by the respective impact events. The average flexural rigidity exhibited by the residual PC type specimens was 9.89 kN-m^2 which is a reduction by 17.3% compared to the intact PC specimens. The rigidity of the residual WC type specimens also showed a reduction in rigidity of 13.4% when compared to the intact WC type specimens.

Comparison with Foam-Core Sandwich Beams

Figure 9 shows the comparison the cardboard core sandwich beams with similar sandwich beams with PIR foam cores tested by Betts et al. (2018b). The figure shows that the sandwich beams perform well compared to beams using more traditional core materials. Both the PC and WC specimens exhibited higher stiffness than all PIR foam core specimens tested in the previous study. However, the PC and WC cores have an average measured density of 136 kg/m^3 and 174 kg/m^3 which is higher than even the most dense foam tested in the study by Betts et al. (2018b) at 96 kg/m^3. Generally, the PC and WC core specimens exhibited a higher ultimate strength than the similar sandwiches with PIR foam core densities of 32 kg/m^3 and 64 kg/m^3, but a lower ultimate strength than the 96 kg/m^3 PIR foam core specimens. Therefore, further research should be performed to examine the shear strength of the face-core interface to have a better understanding of the ultimate load capacity of these structures. Additionally, further research should be performed to understand the freeze-thaw behavior and effect of fire on these structures.

CONCLUSIONS

Twelve sandwich beams with two-layer flax fiber-reinforced polymer faces and corrugated cardboard cores were fabricated and tested under monotonic and impact loads. The main test parameter was the effect of using plain or waxed cardboard for a core material on the flexural behavior of these beams. Additionally, the residual behavior of these sandwich beams after an impact event was investigated. During the tests, the top and bottom face strains and specimen displacement were measured at midspan. Based on the results of the tests, the following conclusions can be drawn:

- Cardboard cores were shown to be comparable with traditional polyisocyanurate (PIR) foam cores. Sandwich beams made with both plain and waxed cardboard cores exhibited a higher stiffness than sandwich beams made with 32 kg/m^3, 64 kg/m^3 and 96 kg/m^3 density PIR cores and a higher ultimate strength than sandwich beams made with the 32 kg/m^3 and 64 kg/m^3 PIR cores.

- There was no significant difference between the load capacity or flexural rigidity of sandwich beams constructed with plain cardboard cores (PC) and waxed cardboard cores (WC). However, the stiffness of the WC specimens was 40.6% higher than the PC specimens.
- An existing design-oriented model was able to predict the static load-deflection behavior of the PC core beams well. The moment-curvature behavior was also predicted well, however the model behavior was softer than the test results.
- Specimens with WC cores and PC cores resisted impact energies of 75% and 37.5% higher than the average static energy to cause failure, respectively.
- Beam strength and stiffness were not adversely affected after being subjected to an impact load. However, the flexural rigidity of both PC and WC type specimens were reduced after being subjected to an impact event. Interestingly, the beam residual strength was higher than the strength of the intact specimens. The current hypothesis is that this increase in strength after an impact event is caused by the densification of the core material during the impact event.
- The interface between the cardboard cores and FFRP faces has a major effect on the overall strength of the panels. Therefore, this is a major design problem for these types of panels and shows that the resin curing temperature, humidity and core surface quality are important parameters. In future studies, to improve the connection between the core and the faces, the core surface should be planed, and a veil should be included in the design.

- Future work on these structures should include interlaminar shear testing of the face-core interface, testing of the effect freeze-thaw on these structures and examining the behavior of these structures when exposed to fire.

ACKNOWLEDGEMENTS

The authors would like to thank Lauren MacDonnell, Yuchen Fu, Jesse Keane, Brian Kennedy and Jordan Maerz for their assistance in the lab. The authors would also like to acknowledge and thank NSERC, Queen’s University, and Dalhousie University for their financial support and Maritime Paper (Dartmouth, NS, Canada) for in-kind contribution.

DATA AVAILABILITY STATEMENT

Some or all data, models, or code that support the findings of this study are available from the corresponding author upon reasonable request.

REFERENCES

Allen, H. G. (1969). *Analysis and Structural Design of Sandwich Panels*. Pergamon Press, Oxford, UK.

Anderson, T., and Madenci, E. (2000). “Experimental investigation of low-velocity impact characteristics of sandwich composites.” *Composite Structures*, 50(3), 239–247.

Andrews, E. W., and Moussa, N. A. (2009). “Failure mode maps for composite sandwich panels subjected to air blast loading.” *International Journal of Impact Engineering*, 36(3), 418–425.

Asdrubali, F., Pisello, A. L., D’Alessandro, F., Bianchi, F., Fabiani, C., Cornicchia, M., and Rotili, A. (2016). “Experimental and numerical characterization of innovative cardboard based panels: Thermal and acoustic performance analysis and life cycle assessment.” *Building and*

Environment, Elsevier Ltd, 95, 145–159.

ASTM. (2005). “ASTM D7136, Standard test method for measuring the damage resistance of a fiber-reinforced polymer matrix composite to a drop-weight impact event.” *Annual Book of ASTM Standards*, 1–16.

ASTM. (2017). “D790, Standard Test Methods for Flexural Properties of Unreinforced and Reinforced Plastics and Electrical Insulating Materials.” *Annual Book of ASTM Standards*.

Atas, C., and Potoglu, U. (2016). “The Effect of Face-Sheet Thickness on Low-Velocity Impact Response of Sandwich Composites with Foam Cores.” *Journal of Sandwich Structures and Materials*, 18(2), 215–228.

Bensadoun, F., Vallons, K. A. M., Lessard, L. B., Verpoest, I., and Van Vuure, A. W. (2016). “Fatigue behaviour assessment of flax-epoxy composites.” *Composites Part A: Applied Science and Manufacturing*, Elsevier Ltd, 82, 253–266.

Betts, D. J., Sadeghian, P., and Fam, A. (2018a). “Impact Behaviour of Sandwich Panels Made of Flax Fiber-Reinforced Bio-Based Polymer Face Sheets and Foam Cores.” *Structures Congress 2018*, 1–7.

Betts, D., Sadeghian, P., and Fam, A. (2017). “Tensile properties of flax frp composites.” *Asia Pacific Conference on FRP in Structures*, International Institute for FRP in Construction, Singapore.

Betts, D., Sadeghian, P., and Fam, A. (2018b). “Experimental Behavior and Design-Oriented Analysis of Sandwich Beams with Bio-Based Composite Facings and Foam Cores.” *Journal of Composites for Construction*, 22(4), 1–12.

Betts, D., Sadeghian, P., and Fam, A. (2018c). “Tensile Preperties of Single Flax Fibres.” *CSCE Annual Conference*, CSCE, Fredericton, NB, Canada, 1–10.

Betts, D., Sadeghian, P., and Fam, A. (2019). “Impact behavior of sustainable sandwich panels with flax FRP faces and cardboard cores." *AEI Conference 2019*, American Society of Civil Engineers, Tysons, Virginia, 1–6.

Betts, D., Sadeghian, P., and Fam, A. (2020). "Erratum for 'Experimental Behavior and Design-Oriented Analysis of Sandwich Beams with Bio-Based Composite Facings and Foam Cores .'" *Journal of Composites for Construction*, 24(1), 08219001–1.

Boria, S., Raponi, E., Sarasini, F., Tirillò, J., and Lampani, L. (2018). "Green sandwich structures under impact: experimental vs numerical analysis." *Procedia Structural Integrity*, Elsevier B.V., 12, 317–329.

Chai, G. B., and Zhu, S. (2011). "A review of low-velocity impact on sandwich structures." *Proceedings of the Institution of Mechanical Engineers, Part L: Journal of Materials Design and Applications*, 225(4), 207–230.

Christian, S. J., and Billington, S. L. (2011). "Mechanical response of PHB- and cellulose acetate natural fiber-reinforced composites for construction applications." *Composites Part B*, Elsevier Ltd, 42(7), 1920–1928.

Codyre, L., Mak, K., and Fam, A. (2016). "Flexural and axial behaviour of sandwich panels with bio-based flax fibre-reinforced polymer skins and various foam core densities." *Journal of Sandwich Structures and Materials*, 1–22.

El Damatty, A. A., Mikhail, A., and Awad, A. A. (2000). "Finite element modeling and analysis of a cardboard shelter." *Thin-Walled Structures*, 28, 145–165.

Entropy Resins. (2013a). *Super SAP ONE Epoxy Resin*. Hayward, CA.

Entropy Resins. (2013b). *Material Safety Data Sheet - Super Sap CLS Hardener*. Hayward, CA.

Entropy Resins. (2015). *Safety Data Sheet - Super Sap ONE Epoxy Resin*. Hayward, CA.

Fam, A., and Sharaf, T. (2010). "Flexural performance of sandwich panels comprising polyurethane core and GFRP skins and ribs of various configurations." *Composite Structures*, Elsevier Ltd, 92(12), 2927–2935.

Ferdous, W., Bai, Y., Ngo, T. D., Manalo, A., and Mendis, P. (2019). "New advancements, challenges and opportunities of multi-storey modular buildings – A state-of-the-art review." *Engineering Structures*, Elsevier, 183(October 2018), 883–893.

Ferdous, W., Manalo, A., and Aravinthan, T. (2017). "Effect of beam orientation on the static behaviour of phenolic core sandwich composites with different shear span-to-depth ratios." *Composite Structures*, Elsevier Ltd, 168, 292–304.

Ferdous, W., Manalo, A., Aravinthan, T., and Fam, A. (2018a). "Flexural and shear behaviour of layered sandwich beams." *Construction and Building Materials*, Elsevier Ltd, 173, 429–442.

Ferdous, W., Manalo, A., Van Erp, G., Aravinthan, T., and Ghabraie, K. (2018b). "Evaluation of an Innovative Composite Railway Sleeper for a Narrow-Gauge Track under Static Load." *Journal of Composites for Construction*, 22(2).

Fraile-Garcia, E., Ferreiro-Cabello, J., Pernia-Espinoza, A., and Martinez-de-Pison, F. J. (2019). "Technical-economic assessment of redesigned reinforced concrete pre-slabs: Incorporating corrugated cardboard." *Structural Concrete*, (August 2018), 1340–1349.

Hristozov, D., Wroblewski, L., and Sadeghian, P. (2016). "Long-term tensile properties of natural fibre-reinforced polymer composites: Comparison of flax and glass fibres." *Composites Part B: Engineering*, Elsevier Ltd, 95, 82–95.

Mak, K., and Fam, A. (2019). "Performance of flax-FRP sandwich panels exposed to different ambient temperatures." *Construction and Building Materials*, Elsevier Ltd, 219, 121–130.

Mak, K., Fam, A., and Macdougall, C. (2015). "Flexural Behavior of Sandwich Panels with Bio-FRP Skins Made of Flax Fibers and Epoxidized Pine-Oil Resin." *Journal of Composites for*

Construction, 19(2003), 1–13.

Mallick, P. K. (2007). *Fiber-Reinforced Composites: Materials, Manufacturing and Design*. CRC Press, NW.

Manalo, A., Surendar, S., van Erp, G., and Benmokrane, B. (2016). “Flexural behavior of an FRP sandwich system with glass-fiber skins and a phenolic core at elevated in-service temperature.” *Composite Structures*, Elsevier Ltd, 152, 96–105.

McCracken, A., and Sadeghian, P. (2018). “Corrugated cardboard core sandwich beams with bio-based flax fiber composite skins.” *Journal of Building Engineering*, Elsevier Ltd, 20(January), 114–122.

Nguyen, M. Q., Jacombs, S. S., Thomson, R. S., Hachenberg, D., and Scott, M. L. (2005). “Simulation of impact on sandwich structures.” *Composite Structures*, 67(2 SPEC. ISS.), 217–227.

Paper & Paperboard Packaging Environmental Council. (2017). “PPEC Factsheet.” <http://www.ppec-paper.com/pdfFiles/factsheets/2017/Packaging/FS03-2017.pdf> (Mar. 8, 2019).

Petras, A., and Sutcliffe, M. P. F. (1999). “Failure mode maps for honeycomb sandwich panels.” *Composite Structures*, 44(4), 237–252.

Pflug, J., Verpoest, I., and Vandepitte, D. (2000). “Folded Honeycomb Cardboard and Core Material for Structural Applications.” *Proceedings of the 5th International Conference on Sandwich Construction*, European Society for Composite Materials, Zurich, Switzerland.

Pflug, J., Xinyu, F., Vangrimde, B., Verpoest, I., Bratfisch, P., and Vandepitte, D. (2002). “Development of a sandwich material with polypropylene / natural fibre skins and paper honeycomb core Development of a sandwich material with polypropylene / natural fibre skins and paper honeycomb core.” *Proceedings of the 10th European Conference on Composites*

Materials, EMAS Publishing.

Plagianakos, T. S., and Papadopoulos, E. G. (2014). "Low-energy impact response of composite and sandwich composite plates with piezoelectric sensory layers." *International Journal of Solids and Structures*, Elsevier Ltd, 51(14), 2713–2727.

Ramesh, M., Palanikumar, K., and Reddy, K. H. (2017). "Plant fibre based bio-composites : Sustainable and renewable green materials." *Renewable and Sustainable Energy Reviews*, Elsevier Ltd, 79(May), 558–584.

Sadeghian, P., Hristozov, D., and Wroblewski, L. (2018). "Experimental and analytical behavior of sandwich composite beams: Comparison of natural and synthetic materials." *Journal of Sandwich Structures and Materials*, 20(3), 287–307.

Schubel, P. M., Luo, J.-J., and Daniel, I. M. (2005). "Low velocity impact behavior of composite sandwich panels." *Composites Part A: Applied Science and Manufacturing*, 36(10), 1389–1396.

Secchi, S., Asdrubali, F., Cellai, G., Nannipieri, E., Rotili, A., and Vannucchi, I. (2016). "Experimental and environmental analysis of new sound-absorbing and insulating elements in recycled cardboard." *Journal of Building Engineering*, Elsevier, 5, 1–12.

Sharaf, T., and Fam, a. (2012). "Numerical modelling of sandwich panels with soft core and different rib configurations." *Journal of Reinforced Plastics and Composites*, 31(11), 771–784.

Sharaf, T., Shawkat, W., and Fam, A. (2010). "Structural performance of sandwich wall panels with different foam core densities in one-way bending." *Journal of Composite Materials*, 44(19), 2249–2263.

Torre, L., and Kenny, J. M. (2000). "Impact testing and simulation of composite sandwich structures for civil transportation." *Composite Structures*, 50(3), 257–267.

Triantafillou, T. C., and Gibson, L. J. (1987). "Failure Mode Maps for Foam-Core Sandwich Beams."

Materials Science and Engineering, 95, 37–53.

Vitale, J. P., Francucci, G., Xiong, J., and Stocchi, A. (2017). "Failure mode maps of natural and synthetic fiber reinforced composite sandwich panels." *Composites Part A: Applied Science and Manufacturing*, Elsevier Ltd, 94, 217–225.

Zhu, D., Shi, H., Fang, H., Liu, W., Qi, Y., and Bai, Y. (2018). "Fiber reinforced composites sandwich panels with web reinforced wood core for building floor applications." *Composites Part B: Engineering*, Elsevier, 150(April), 196–211.

Zhu, S., and Chai, G. B. (2013). "Damage and failure mode maps of composite sandwich panel subjected to quasi-static indentation and low velocity impact." *Composite Structures*, Elsevier Ltd, 101, 204–214.

Table 1. Test Matrix

Specimen Group	**Quantity**	**Core Type**	**Test Type**
2FL-PC-S	3	Plain Cardboard	Static
2FL-PC-D	3	Plain Cardboard	Dynamic (Impact)
2FL-WC-S	3	Waxed Cardboard	Static
2FL-WC-D	3	Waxed Cardboard	Dynamic (Impact)

Table 2. Monotonic Test Results

Specimen	Mass, kg	Ultimate Load, kN	Max Deflection, mm	Specific Strength, kN/kg	Stiffness, N/mm	Ultimate Moment, kN-m	Max Curvature, 1/km	Flexural Rigidity, kN-m^2	Failure Mode
2FL-PC-S-1	2.844	2.91	15.4	1.02	271.0	0.81	115	10.39	CW
2FL-PC-S-2	2.823	4.26	22.6	1.51	263.2	1.19	169	11.27	CW
2FL-PC-S-3	2.769	4.51	24.8	1.63	236.3	1.26	132	14.21	CW
AVE	2.812	3.89	20.9	1.4	256.9	1.09	139	11.96	
SD	0.038	0.86	4.9	0.3	18.2	0.24	27	2.00	
2FL-WC-S-1	3.267	3.96	17.9	1.21	348.6	1.10	129	11.86	CW
2FL-WC-S-2	3.258	2.10	14.3	0.64	344.1	0.59	53	12.46	CW
2FL-WC-S-3	3.456	5.84	38.2	1.69	390.9	1.63	254	13.92	CS
AVE	3.327	3.96	23.5	1.2	361.2	1.11	145	12.74	
SD	0.112	1.87	12.9	0.5	25.8	0.52	101	1.06	

* *CW = Compression Face Wrinkling; CS = Core Shear, AVE = Average, SD = Standard Deviation*

Table 3. Results of Monotonic Design Oriented Model

Specimen Group	Ultimate Load, kN	Max Deflection, mm	Stiffness, N/mm	Ultimate Moment, kN-m	Max Curvature, 1/km	Rigidity, kN-m^2	Failure Mode
Model	4.72	23.9	262.3	1.32	218	8.02	TR/CC
PC Tests	3.89	20.9	256.9	1.09	139	11.96	CW
PC-Model Ratio	0.82	0.88	0.98	0.82	0.63	1.49	N/A

Table 4. Impact Test Results

Specimen	Mass, kg	Drop Height, mm	Absorbed Energy, J	Specific Absorbed Energy, J/kg	Maximum Deflection, mm	Maximum Bottom Face Strain, mm/mm	Minimum Top Face Strain, mm/mm	Calculated Stiffness, N/mm	Damping Ratio, %
2FL-PC-D-1	2.81	614	62.72	22.30	18.5	0.0073	-0.0077	277	8.9
2FL-PC-D-2 †	2.78	1075	Break	Break	N/A	N/A	N/A	N/A	N/A
2FL-PC-D-3 *	2.75	845	86.32	31.39	23.3	0.0096	-0.0087	N/A	N/A
2FL-WC-D-1	3.36	614	62.72	18.69	18.6	0.0071	-0.0055	256	11.4
2FL-WC-D-2 †	3.32	1517	Break	Break	N/A	N/A	N/A	N/A	N/A
2FL-WC-D-3	3.32	1075	109.81	33.07	25.6	0.0086	-0.0060	284	8.7

* *String potentiometer failed after maximum deflection*

† *Specimen experienced ultimate failure*

Table 5. Residual Monotonic Test Results

Specimen	Mass, kg	Ultimate Load, kN	Max Deflection, mm	Specific Strength, kN/kg	Stiffness, N/mm	Ultimate Moment, kN-m	Max Curvature, 1/km	Flexural Rigidity, kN-m^2	Failure Mode
2FL-PC-D-1-R	2.799	5.67	32.3	2.02	285.2	1.58	275	9.80	CC
2FL-PC-D-3-R	2.743	6.84	49.7	2.49	268.2	1.91	357	9.99	CC
AVE	2.771	6.25	41.0	2.26	276.7	1.75	316	9.89	
SD	0.039	0.83	12.3	0.33	12.0	0.23	58	0.13	
2FL-WC-D-1-R	3.359	6.81	41.2	2.03	353.3	1.90	350	10.40	CC
2FL-WC-D-3-R	3.315	6.63	40.8	2.00	336.7	1.85	309	11.67	CC
AVE	3.337	6.72	41.0	2.01	345.0	1.88	329	11.03	
SD	0.031	0.12	0.2	0.02	11.8	0.03	29	0.90	

* *CC = Compression Face Crushing, AVE = Average, SD = Standard Deviation*

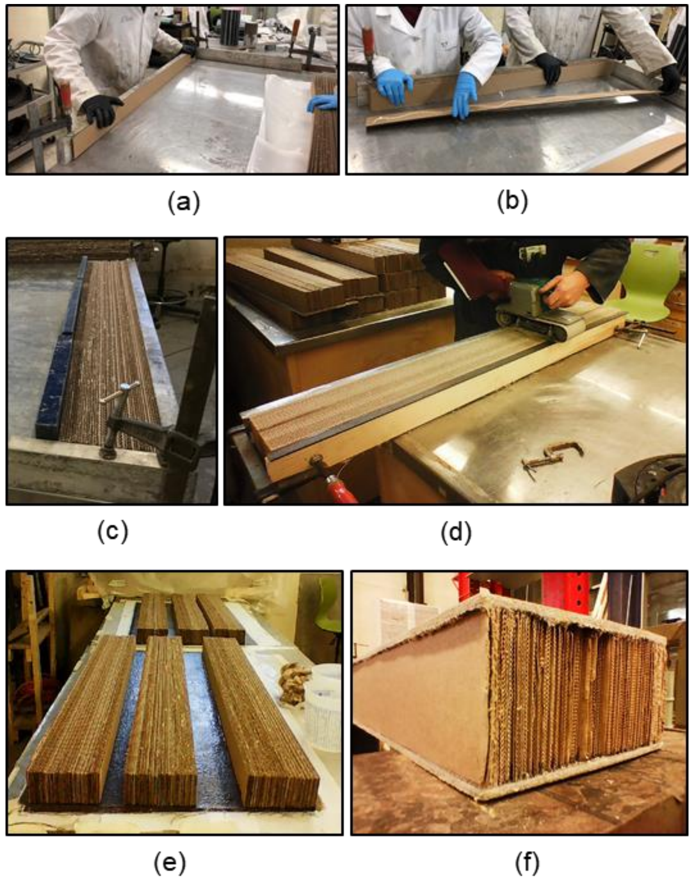

Figure 1. Specimen Fabrication: (a) Placement of First Cardboard Strip; (b) Gluing and Placement of Subsequent Cardboard Strips; (c) Glue Drying on Plain Cardboard Core; (d) Sanding Top of Cardboard Core (e) Cardboard Cores Placed on FFRP Face and; (f) Finished Specimen. [Photos courtesy of Yuchen Fu and Dillon Betts]

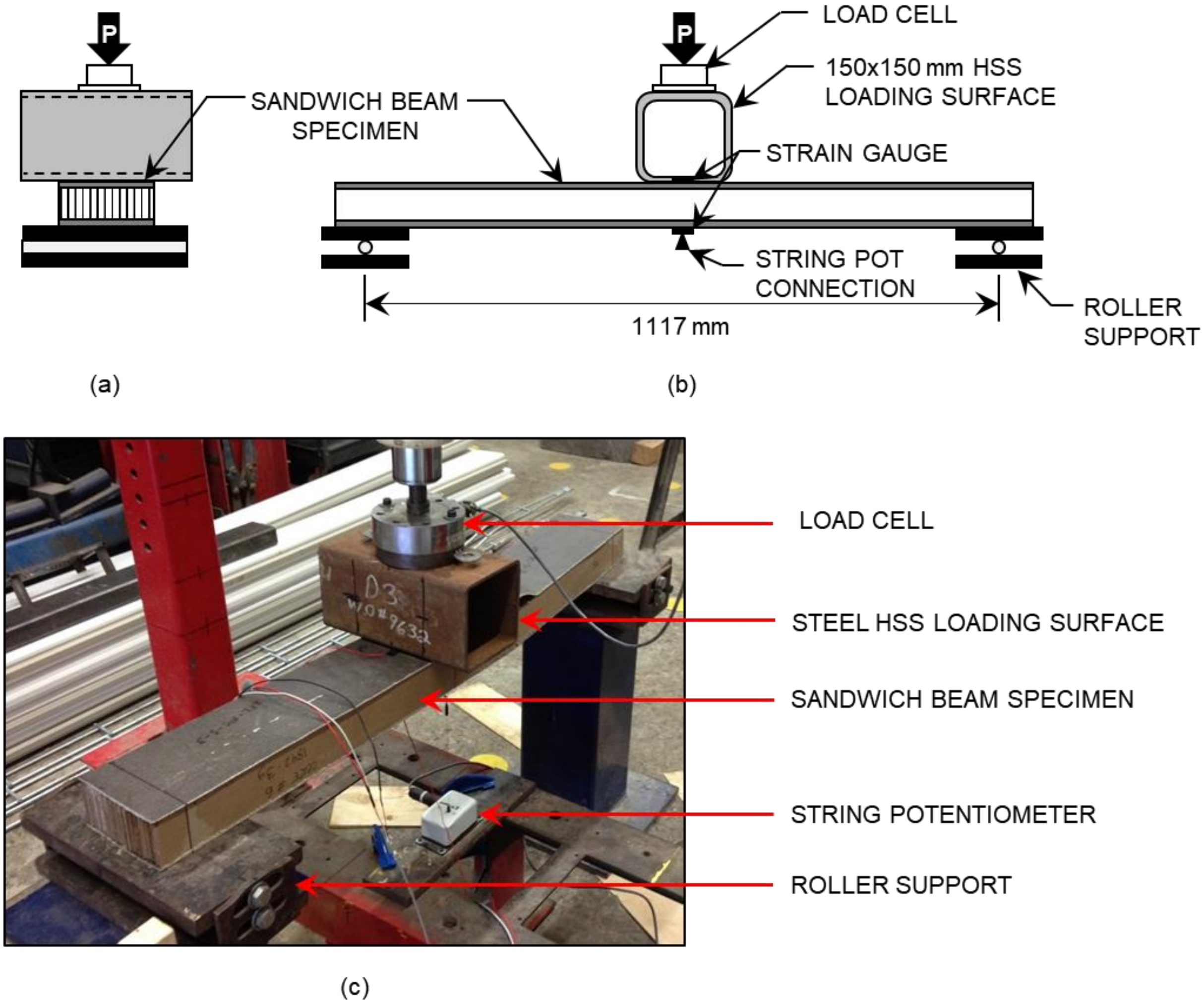

Figure 2. Monotonic Test Set-up (a) End View Schematic; (b) Side View Schematic and; (c) Photo.

[Photo courtesy of Dillon Betts]

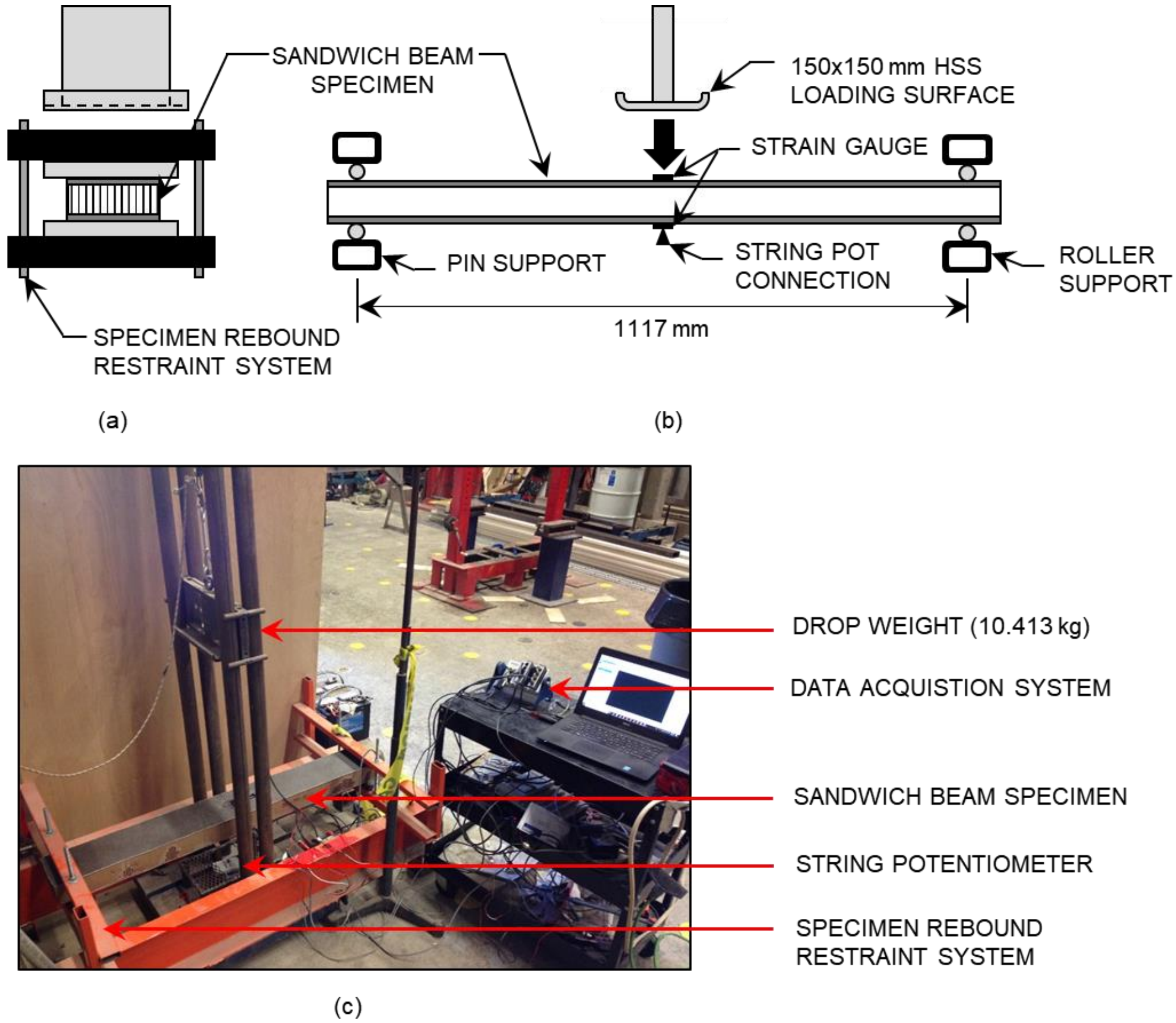

Figure 3. Impact Test Set-up (a) End View Schematic; (b) Side View Schematic and; (c) Photo.

[Photo courtesy of Dillon Betts]

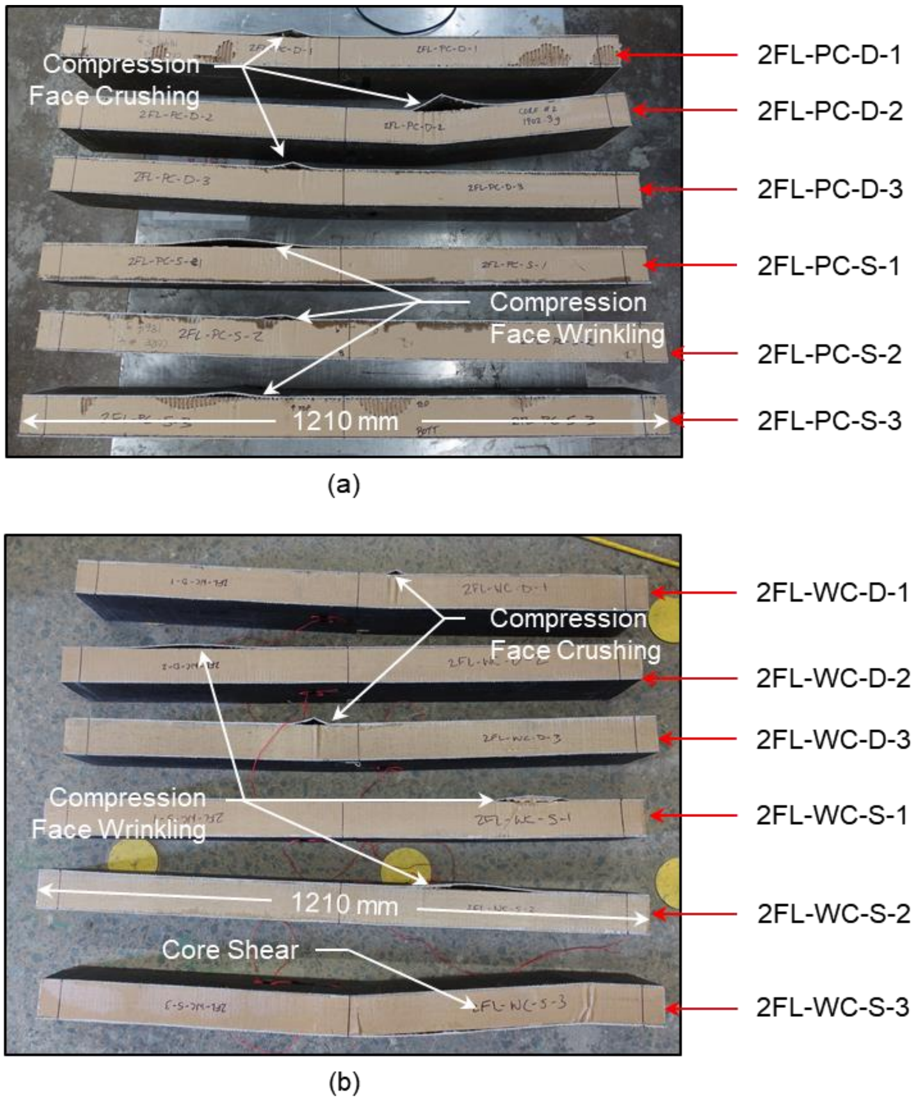

Figure 4. Failed Specimens (a) Plain Core Specimens and; (b) Waxed Core Specimens (Note that specimens 2FL-WC-D-2 and 2FL-PC-D-2 failed under impact and were not tested for residual properties). [Photos courtesy of Dillon Betts]

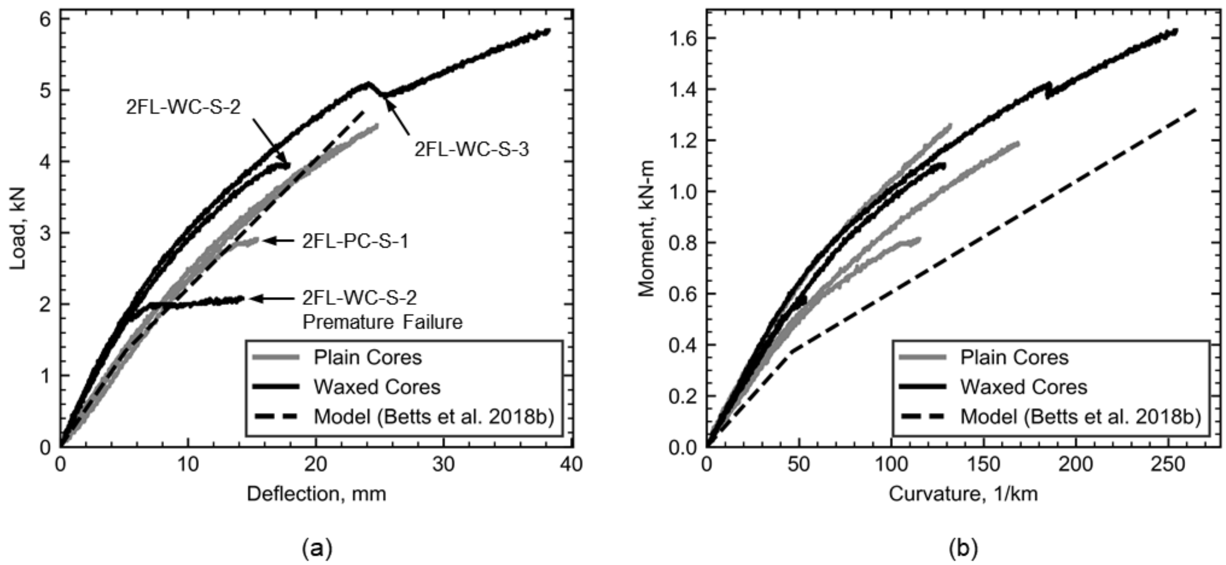

Figure 5. Test Results of Monotonic Three-Point Bending Tests (a) Load-Deflection and; (b) Moment-Curvature.

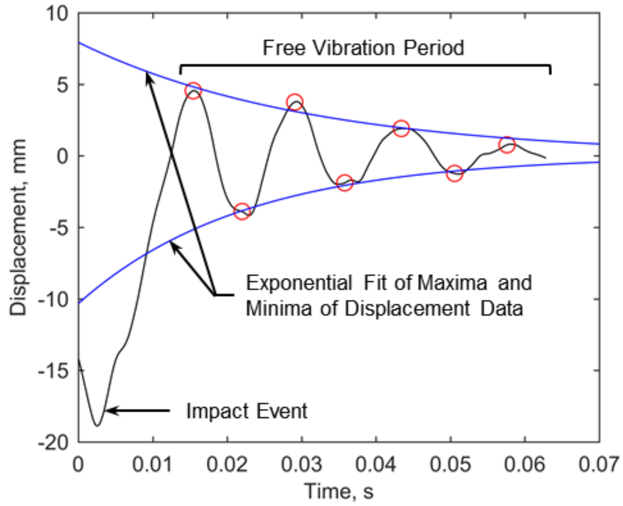

Figure 6. Specimen 2FL-PC-D-1 – Damping Ratio Calculation.

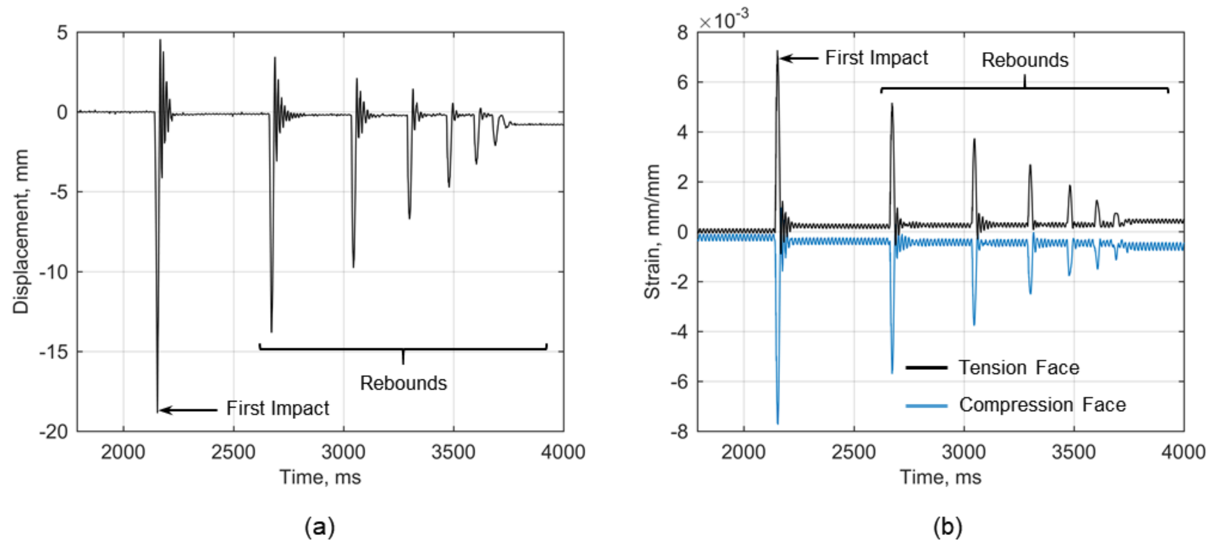

Figure 7. Specimen 2FL-PC-D-1 Impact Test Data (a) Midspan Displacement vs. Time and; (b) Face Strain at Midspan vs. Time.

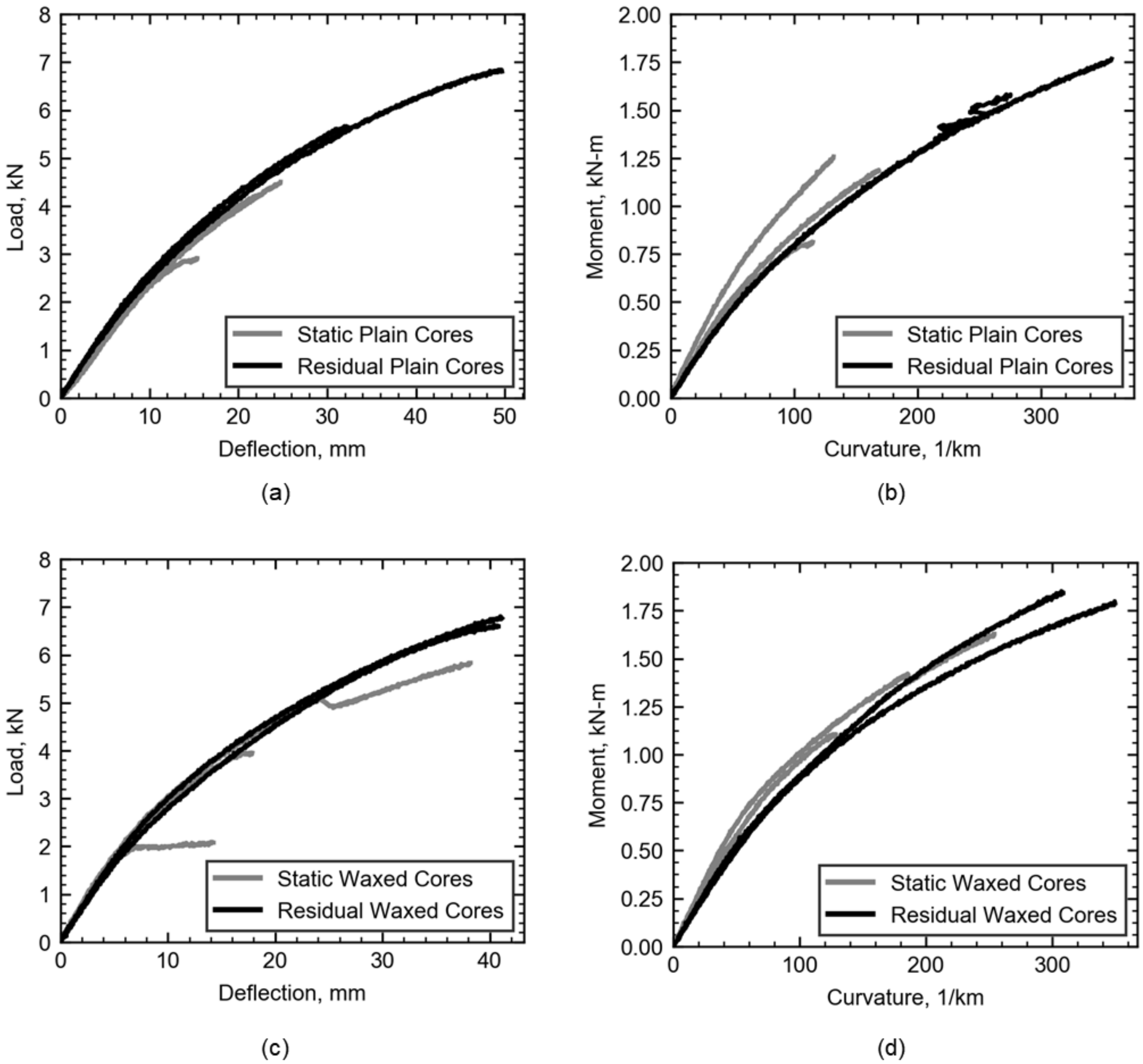

Figure 8. Comparison of the Residual Properties of Cardboard Core Sandwich Beams and Intact Static Properties (a) Load-Deflection of Plain Core Specimens; (b) Moment-Curvature of Plain Core Specimens; (c) Load-Deflection of Waxed Core Specimens and; (d) Moment-Curvature of Waxed Core Specimens.

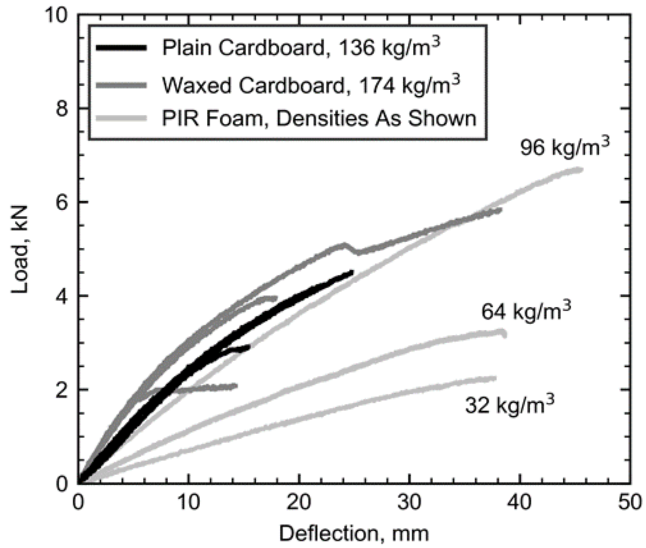

Figure 9. Load-Deflection Comparison of Plain and Waxed Cardboard Core FFRP-Sandwich Beams with Foam Core FFRP-Sandwich Beams – PIR Foam Core Data from Betts et al. (2018b)